Violations of Jeffery's theory in the dynamics of nanographene in shear flow

Gravelle, Simon; Kamal, Catherine; Botto, Lorenzo

DOI
10.1103/PhysRevFluids.6.034303

Publication date
2021

Document Version
Final published version

Published in
Physical Review Fluids

Violations of Jeffery's theory in the dynamics of nanographene in shear flow

Simon Gravelle and Catherine Kamal
School of Engineering and Material Science, Queen Mary University of London, London, United Kingdom

Lorenzo Botto*
Process and Energy Department, 3ME Faculty of Mechanical, Maritime and Materials Engineering, TU Delft, Delft, The Netherlands

(Received 11 September 2020; accepted 1 March 2021; published 26 March 2021)

Using molecular dynamics simulations we investigate the shear-induced rotational dynamics of a Brownian nanographene (hexabenzocoronene) freely suspended in a liquid. We demonstrate that, owing to a finite hydrodynamic slip at the molecular surface, these flat molecules tend to align with a constant orientation angle instead of performing the classical periodic orbits predicted by Jeffery's theory. Results are extracted for different Péclet numbers and compared to the predictions by a theory developed for a rigid axisymmetric particle with orientation confined to the flow-gradient plane. The theory is based on the resolution of a one-dimensional Fokker-Planck equation for the angle φ made by one of the particle's diameters with the flow direction. Remarkably, our results show that the essential features of the three-dimensional orientational statistics of the nanographene are captured by the one-dimensional model, given that the hydrodynamic velocity is closed in terms of the slip length λ. Finally, we explore the situation in which multiple nanographenes are suspended in the liquid, and show that slip results in a reduction in specific viscosity.

DOI: 10.1103/PhysRevFluids.6.034303

I. INTRODUCTION

The competition between Brownian motion and shear-induced orientation is a fundamental mechanism that determines the dynamical state of anisotropic soft matter under flow. This competition controls, for instance, the flow properties of liquid crystals, polymers, and colloidal suspensions [1–4], and has been used as a tool to probe the morphology of macromolecules [5,6].

The rotational dynamics of anisotropic colloidal particles or solute molecules in shear flow is well known for objects satisfying the hydrodynamic no-slip boundary condition [7,8]. The widely applied theory of Jeffery predicts that at high Péclet numbers (Pe), a no-slip rigid axisymmetric particle rotates continuously about one of its axes, completing full periodic rotations [9]. Such prediction also applies when the slip length λ, characterizing the propensity of the fluid to slip at the fluid-solid boundaries, remains smaller than the particle thickness $2b$, except that the period of the rotations is reduced with respect to the no-slip case [10,11]. However, our recent results suggest that Jeffery's theory fails to predict the rotational dynamics of a plate-like particle in the case of larger slip lengths: for λ larger than $2b$, the particle is predicted to find an equilibrium orientation at a small angle with the flow without rotating [12]. This prediction applies to a rigid particle that is constrained to move in the flow-gradient plane [i.e., quasi-two-dimensional (quasi-2D) system], and its applicability to flat molecular solutes poses a fundamental challenge [13]: first, Brownian

*l.botto@tudelft.nl

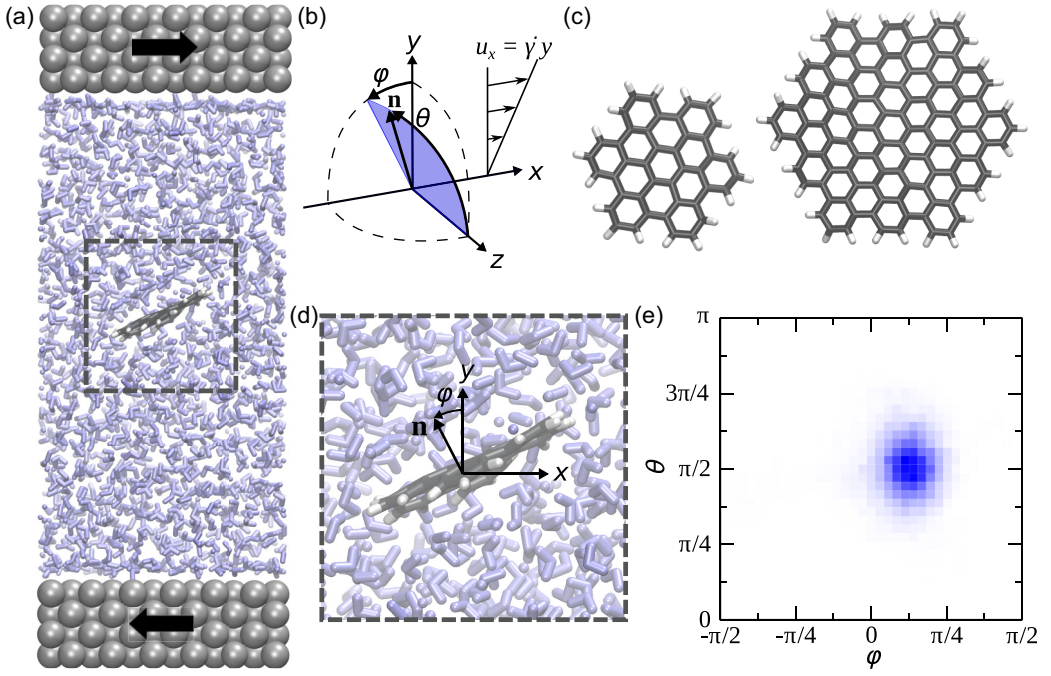

FIG. 1. (a) Snapshot of the molecular dynamics system, with a single HBC immersed in water (in blue). Gray layers at the top and bottom are the shearing walls. (b) Coordinate system with Euler angles φ and θ; when the normal $\mathbf{n}$ is in the flow-gradient plane, $\theta = \pi/2$. $\dot{\gamma}$ is the shear rate. (c) HBC of formula $C_{42}H_{18}$ (left), and molecule of formula $C_{114}H_{30}$ (right). Carbon atoms are in dark gray and hydrogen atoms in white. (d) Zoom on the HBC inclined by an angle φ with respect to the flow. (e) Angular probability distribution $p(\varphi, \theta)$ for a single HBC and $\dot{\gamma} = 50\ \text{ns}^{-1}$. Dark blue indicates high probability.

fluctuations induce motions of the molecules out of the flow-gradient plane and, second, these molecules are flexible. These effects can alter the orientational probability distribution in, so far, unknown ways. Hence, the characterization of the full orientational probability distribution of molecules with three-dimensional (3D) trajectories is necessary.

In this paper, using molecular dynamics simulations, we study the dynamics of hexabenzocoronene (HBC) in a shear flow. HBCs are a class of graphenes of lateral length in the nanometer range (Fig. 1). Owing to dispersion properties and shape similar to larger graphene molecules, HBCs are excellent model systems for studying the dynamics of graphene in solution [14]. Furthermore, the study of these polycyclic aromatic molecules can shed light into the dynamics of the more complex molecules that appear ubiquitously whenever organic matter is decomposed or processed (e.g., asphaltenes). We show that, at large Pe numbers, HBC displays arrested rotational dynamics in three dimensions in keeping with the 2D theory. The dynamics is rationalized by solving a Fokker-Planck equation for the orientational probability distribution of a rigid particle with slip. The model neglects degrees of freedom associated to motions out of the flow-gradient plane, but predicts, however, the observed orientational statistics with only a slight overestimation of the degree of alignment. As an example of the impact of this microscopic phenomenon on macroscopic quantities, we demonstrate that, by affecting the HBC orientation, slip leads to a significant reduction of the specific effective viscosity of liquid solvents containing several suspended HBCs. The fact that a large number of 2D nanomaterials have significant slip lengths (for atomically smooth surfaces, λ can exceed several nanometers [15,16]) makes these results of broader significance for understanding the dynamics of 2D nanomaterials, including graphene, hexagonal boron nitride, and molybdenum disulfide.

II. METHODS AND RESULTS

A. Single solute particle

We first perform molecular dynamics simulations of a single HBC (henceforth referred to as particle when discussing microhydrodynamic modeling aspects) freely suspended in a linear shear flow $u_x = \dot{\gamma} y$ using LAMMPS [17]. The all-atom GROMOS force field was used for the aromatic molecules [18], the TIP4P/2005 model was used for water [19], and crossed parameters were calculated using the Lorentz-Berthelot mixing rule. Long-range Coulombic interactions were computed using the particle-particle particle-mesh (PPPM) method [20,21]. Shear was imposed to the fluid using two moving walls (Fig. 1). Periodic boundary conditions were used along the three orthogonal directions. A temperature $T = 300$ K was maintained using a Berendsen thermostat applied only to the solvent, and only to the degrees of freedom perpendicular to the direction of the flow. Data were recorded after an equilibrium step of duration 1 ns. See Supplemental Material [22] for more details about the simulation [23–25].

The orientation of the normal **n** to the center of the HBC as given by the Euler angles θ and φ was measured [Fig. 1(b)]. The results show that with a shear rate $\dot{\gamma} = 50\,\mathrm{ns}^{-1}$, the HBC aligns with the flow near the angles $\varphi_c = \pi/8$ and $\theta_c = \pi/2$ [Fig. 1(e)], performing small fluctuations about these angles due to thermal motions. The value of φ_c is small but finite, in keeping with a theory developed for plate-like particles constrained to move in the flow-gradient plane [12]. According to this theory, the arrested dynamics is a consequence of stress redistribution induced by the slip at the fluid-solid boundary, and can be understood by considering the values of the torque applied by the fluid on the particle when the particle is kept aligned with the flow [$T(\varphi = 0, \theta = \pi/2)$] or perpendicular to the flow [$T(\pi/2, \pi/2)$]. It can be shown that $T(\pi/2, \pi/2)$ is always negative regardless of the value of the slip length λ. In this case, the torque tends to rotate the particle clockwise (in the direction of the vorticity). For a no-slip particle, $T(0, \pi/2)$ is also negative. However, if the slip length λ is larger than the particle half-thickness b, $T(0, \pi/2)$ is positive. Therefore, for a particle with large hydrodynamic slip, there is an equilibrium angle φ_c, with $0 < \varphi_c < \pi/2$. It can be shown that φ_c is given by [12]

$$\tan \varphi_c = \sqrt{\frac{-T(0, \pi/2)}{T(\pi/2, \pi/2)}}. \tag{1}$$

For the HBCs, we find using molecular dynamics that $T(0, \pi/2) = (-2.5 \pm 0.7)$ Kcal/mol and $T(\pi/2, \pi/2) = (17.5 \pm 0.7)$ Kcal/mol, and therefore one gets $\varphi_c = 0.36 \pm 0.06$ from Eq. (1), in good agreement with the molecular dynamics results of Fig. 1(e).

To assess the relative importance of the Brownian and hydrodynamic contributions to the dynamics, we quantify the Péclet number $\mathrm{Pe} = \dot{\gamma}/D_r$, where D_r is the rotational diffusion coefficient associated with the rotation of the HBC about one of its diameters. We evaluate D_r using molecular dynamics simulations, by measuring the rotational relaxation time from autocorrelation function analysis [26,27]. See Supplemental Material [22] for details about the rotational diffusion coefficient measurement. We find a correlation time $\tau = (190 \pm 20)$ ps and $D_r = 1/6\tau = (0.9 \pm 0.1)\ \mathrm{ns}^{-1}$. The measured value for D_r is remarkably close to the estimate $D_r \approx 3k_B T/32\eta a^3 \approx 0.88\ \mathrm{ns}^{-1}$ for an infinitely thin rigid disk of radius a, where k_B is the Boltzmann constant, T the temperature [28]. For the HBC, we use $a = 8$ Å as the effective radius. Here the effective radius corresponds to the actual radius of the HBC (i.e., the distance between the center of the hydrogen atoms and the center of the HBC) plus the effective radius of the hydrogen atoms [i.e., the radius of the hydrogen atoms as seen by the water molecules, which is given by the parameters of the Lennard-Jones potential [Fig. (S1) [22]]. The good agreement between the continuum prediction and molecular dynamics for the value of D_r is all the more striking given that the HBC is flexible. For the simulation presented in Fig 1(e), $\dot{\gamma} = 50\ \mathrm{ns}^{-1}$, therefore $\mathrm{Pe} = 62$. Standard rheometers are typically limited to shear rate $\dot{\gamma} < 10^5\ \mathrm{s}^{-1}$ [29,30], and a value of 62 for the Péclet number is not accessible using HBCs in water.

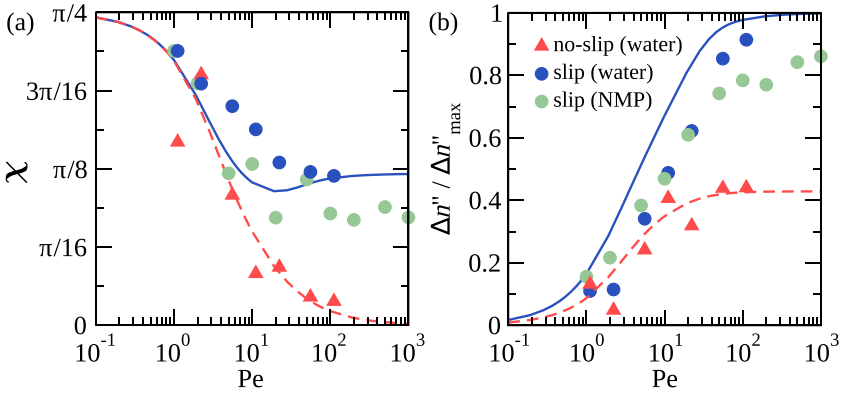

FIG. 2. (a) Average orientation angle χ [Eq. (2)] and (b) degree of alignment $\Delta n''/(\Delta n''_{\max})$ [Eq. (3)] for $N = 1$: slip HBC in water (blue disks); slip HBC in NMP (green disks); no-slip HBC in water (red triangles). Lines are theory [Eqs. (4)–(6)] with $k_e = 0.4i$ (full blue line) and $k_e = 0.4$ (dashed red line). An imaginary value for the effective aspect ratio k_e is associated to slip particles. For a particle with its normal near $\theta = \pi/2$, χ is approximately equal to $\langle\varphi\rangle$ when χ is small.

However, $\mathrm{Pe} = 62$ is accessible experimentally using solute particles or molecules of micrometric lengths [31].

To present statistical observables that can be compared directly with experiments, we compute the so-called average orientation angle χ and the degree of alignment $\Delta n''/\Delta n''_{\max}$. These two quantities are often used in rheo-optical studies [31,32]. The average orientation angle is defined as

$$\chi = \frac{1}{2}\arctan\left(\frac{\langle \sin^2\theta\ \sin 2\varphi\rangle}{\langle \sin^2\theta\ \cos 2\varphi\rangle}\right). \tag{2}$$

This expression gives $\chi = 0$ for a particle aligned near $\varphi = 0$. For $\mathrm{Pe} \geqslant 62$ we obtain $\chi \approx 0.3$, indicating an average alignment of the HBC at a nonzero angle [blue disks in Fig. 2(a)]. The degree of alignment is

$$\frac{\Delta n''}{\Delta n''_{\max}} = \sqrt{\langle \sin^2\theta\ \sin 2\varphi\rangle^2 + \langle \sin^2\theta\ \cos 2\varphi\rangle^2}. \tag{3}$$

In rheo-optical studies, $\Delta n''$ is the magnitude of the dichroism and $\Delta n''_{\max}$ its value in the fully aligned state. Essentially, the degree of alignment is related to the variance of χ, i.e., the spread of the orientation from its average value. For large Pe, we find $\Delta n''/\Delta n''_{\max} \to 1$, indicating that the variance of the orientational distribution around the average angle χ is relatively small [blue disks in Fig. 2(b)]. Expectedly, $\Delta n''/\Delta n''_{\max} \to 0$ as Pe decreases, because of the randomizing effect of Brownian fluctuations. We compare in Fig. 3 the angular distribution $p(\varphi, \theta)$ for intermediate and relatively large Péclet numbers: $\mathrm{Pe} = 62$ [Fig. 3(a)] and $\mathrm{Pe} = 6.2$ [Fig. 3(b)]. For $\mathrm{Pe} = 6.2$, the HBC escapes the hydrodynamic potential well several times during the simulation. It explores the full orientational space, but spends the largest fraction of the rotational period oriented near $\varphi_c = \pi/8$.

To rationalize the molecular dynamics (MD) predictions, we compare the MD data with a model for the orientational distribution function that neglects the dependence on θ. This assumption is justified for a rigid axisymmetric particle in a shear flow, for which variations in φ are dynamically decoupled from variations in θ [33], and for which the diffusion tensor is diagonal [34]. The probability p of finding a rigid axisymmetric particle at a certain orientation angle φ in response to hydrodynamic and Brownian stresses is given by a Fokker-Planck (Smoluchowski) equation [35].

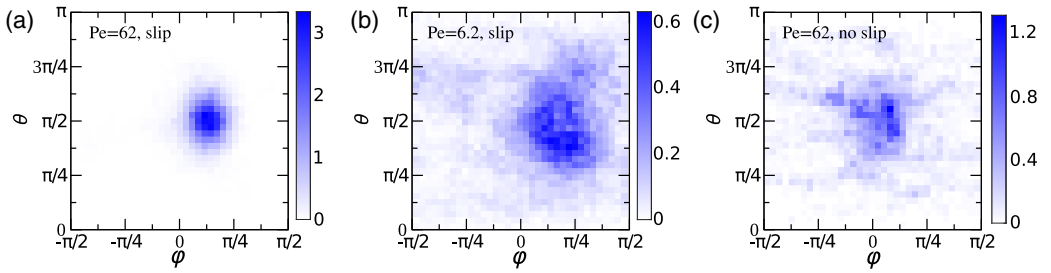

FIG. 3. (a), (b) Angular probability distribution $p(\varphi, \theta)$ for a single slip HBC with Pe = 62 (a) and Pe = 6.2 (b). (c) $p(\varphi, \theta)$ for a single no-slip HBC with Pe = 62.

With just one degree of freedom, this equation simplifies to [13]

$$\frac{\partial p}{\partial t} = \frac{\partial}{\partial \varphi}\left(D_{\mathrm{r}}\frac{\partial p}{\partial \varphi} - \Omega(\varphi)\dot{\gamma}\, p\right), \tag{4}$$

where $\Omega(\varphi)\dot{\gamma}$ is the hydrodynamic angular velocity. A classical solution due to Bretherton for two-dimensional axisymmetric particles rotating in the flow-gradient plane provides an exact expression for $\Omega(\varphi)$ in terms of a single scalar parameter k_{e}, the effective aspect ratio [33,36]:

$$\Omega(\varphi) = -\left(k_{\mathrm{e}}^2 \cos\varphi^2 + \sin\varphi^2\right)\Big/\left(1 + k_{\mathrm{e}}^2\right). \tag{5}$$

The parameter k_{e} is defined as the ratio [7]

$$k_{\mathrm{e}} = \sqrt{\frac{T(0)}{T(\pi/2)}} \tag{6}$$

of the hydrodynamic torques on a particle held fixed, respectively, parallel ($\varphi = 0$) and perpendicular ($\varphi = \pi/2$) to the flow for $\theta = \pi/2$. In absence of slip, $T < 0\ \forall\ \varphi$, therefore, $k_{\mathrm{e}} \in \mathbb{R}$. In this case, $\Omega < 0\ \forall\ \varphi$ and the solution of Eq. (5) yields periodic trajectories known as Jeffery's orbits [9]. This is the case classically studied in colloidal hydrodynamics. However, the possibility that $T(0)/T(\pi/2)$ is negative exists. In a previous work [12] we analyzed the case of a bidimensional plate-like particle with surface slip length λ. We found that while the sign of $T(\pi/2)$ is essentially independent of λ, $T(0)$ changes sign when λ becomes sufficiently large in comparison with the particle half-thickness b. As a consequence, k_{e} becomes a purely imaginary complex number [12]. In this case, Eq. (5) admits the (time-independent) stable solution $\varphi_{\mathrm{c}} \approx \arctan(|k_{\mathrm{e}}|)$. Therefore, the value of λ alters the nature of Eq. (4) and, in turn, the rotational dynamics at finite Pe. While the theory was developed for a rigid particle with orientation confined to the flow-gradient plane, here we demonstrate its applicability to a flexible molecule that rotates in the three-dimensional space.

By computing $T(0)$ and $T(\pi/2)$ for HBC in water with $\theta = \pi/2$, we find $k_{\mathrm{e}} = 0.41i$. See Supplemental Material [22] for details about the effective aspect ratio measurement. Solving Eqs. (4) and (5) with this value of k_{e}, and using the corresponding probability distribution p to calculate the averages in Eqs. (2) and (3), gives values of χ and $\Delta n''/\Delta n''_{\mathrm{max}}$ that are in unexpectedly good agreement with the MD results [blue lines in Figs. 2(a) and 2(b)]. While there are some differences between the model and the MD data, the dependence of χ on Pe and the characteristic value of χ for Pe $\to \infty$ are essentially captured; the degree of orientation is only slightly overestimated. That a model developed for a particle orientation confined to the flow-gradient plane can capture essential features of the 3D rotational dynamics has been discussed before in the context of asymmetric particles following Jeffery's orbits [13,37]. The model [Eqs. (4)–(6)] was developed for a rigid particle, but HBCs have a finite bending rigidity, which we measure to be $B = 1.1$ eV. See Supplemental Material [22] for details about the bending rigidity measurement [38,39]. The

theoretical predictions are expected to hold only for the range of parameters for which the molecule behaves approximately as a rigid object.

To evaluate the range of parameters for which the HBC can be considered rigid, one might consider the balance of elastic forces, of characteristic magnitude $\sim B/a$, and viscous forces $\sim\eta\dot{\gamma}a^2$. Equating these two contributions yields the following buckling threshold [40]:

$$\hat{\sigma} = \frac{B}{\dot{\gamma}\eta a^3} \sim 1, \tag{7}$$

where η is the fluid viscosity. The parameter σ^{-1} is akin to the viscoelastic number commonly used for fibers, except for the different scaling of elastic forces with respect to the fiber length [41]. For the HBC, assuming $a = 8$ Å, we get $\hat{\sigma} \leqslant 1$ for $\dot{\gamma} \geqslant 400$ ns^{-1}. In keeping with Eq. (7), in the present simulations (in which $\dot{\gamma} \leqslant 100$ ns^{-1}), the HBC has the same rotational statistics of a rigid molecule. To further test the validity of Eq. (7), we performed simulations with a larger molecule of formula $C_{114}H_{30}$, effective radius $a = 12.5$ Å, and measured rotational diffusion coefficient $D_r = (0.16 \pm 0.05)$ ns^{-1} [Fig. 1(c)]. Two situations are considered: either the $C_{114}H_{30}$ molecule is free to deform, or it is constrained to move according to a rigid body motion. We observe no significant statistical difference between the flexible and the rigid molecules for $\dot{\gamma}$ as high as 100 ns^{-1}, corresponding to $\hat{\sigma} \approx 1$ (Fig. S2 [22]). This observation contradicts Eq. (7). The explanation for this is that Eq. (7) assumes that viscous forces scales as $\sim\eta\dot{\gamma}a^2$. However, compressive hydrodynamic stresses of $O(\eta\dot{\gamma}a^2)$ occur only when the particle is oriented along the compressional axis of the flow. This configuration does not occur when $\lambda > 2b$ (in this case the orientation is along the flow, or slightly inclined along the extensional axis). In addition, the reduced friction at the fluid-particle surface leads to reduced viscous forces. In the case of a rigid platelet with half-length a, viscous forces are reduced by a factor $1/(1 + 4\lambda/\pi a)$ [12]. Assuming that the same correction applies to disk-shaped HBC, and using $\lambda = 10$ nm [15] and $a = 8$ Å, slip is expected to reduce the viscous forces by a factor 0.06. As a consequence, for $\lambda > 2b$, compressive stresses are much smaller than $\sim\eta\dot{\gamma}a^2$, and thus Eq. (7) overestimates the buckling threshold. Therefore, slip has an effect on the deformation of a solute molecule by changing the range of hydrodynamic compressive stresses the molecule experiences.

Aside from rigidity, the continuum assumptions (4)–(6) rely on may break down for a solvent composed of relatively large molecules (larger than those of water). We perform MD simulations using, as solvent, N-methyl-2-pyrrolidone (NMP), whose molecules have more complex shapes and are larger than those of water. See Supplemental Material [22] for details about the simulation. Understanding the hydrodynamics of molecules or nanoparticles in NMP is particularly relevant because NMP is considered an excellent dispersant for carbon nanomaterials [14,42]. We found that the results for NMP are qualitatively similar to those obtained with water, with the HBC in NMP also displaying arrested dynamics [Figs. 2(a) and 2(b)]. The main difference between water and NMP is a slightly reduced value of χ for Pe > 4, and a reduced value of $\Delta n''/\Delta n''_{\max}$ for Pe > 10, confirming that the solvent's molecular size and shape affect the HBC average orientation. The size and shape of the solvent molecules are also known to affect the rotational diffusion coefficient of suspended molecules (as suggested, for example, by rotational relaxation time experiments [43]). In agreement with this observation, we measure $D_r = (0.1 \pm 0.1)$ ns^{-1} for the HBC in NMP, a value much smaller than the one for water [$D_r = (0.9 \pm 0.1)$ ns^{-1}]. Such reduction, by a factor $1/9$, cannot be explained by the difference in bulk viscosity of the two fluids ($\eta = 0.855$ mPa s for TIP4P/2005 water at 300 K [44], and $\eta = 1.6$ mPa s for NMP [45]), and is likely to originate from the different shapes and sizes of the solvent molecules.

To demonstrate that the suppression of rotation in the case of HBC is actually caused by hydrodynamic slip, we performed simulations with a no-slip HBC. The no-slip boundary condition was enforced by modifying the energy of interaction between the carbon atoms of the HBC and the oxygen atoms of the water molecules. See Supplemental Material [22] for details about the enforcement of the no-slip boundary condition [46]. At large Pe number, the no-slip HBC

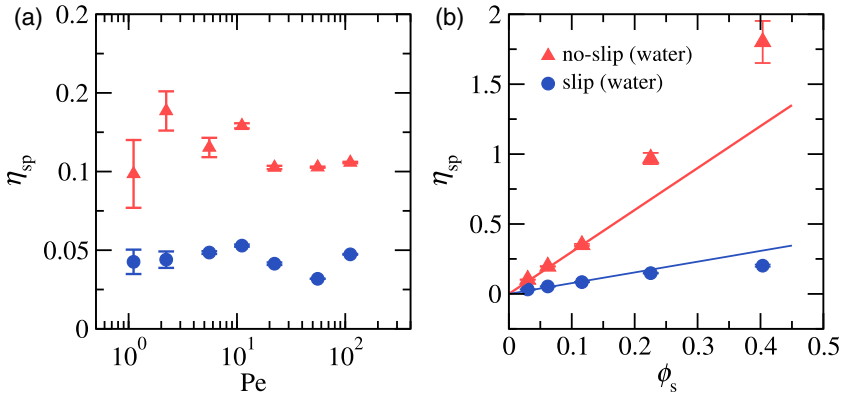

FIG. 4. (a) Specific viscosity as a function of Pe for a single slip HBC in water (blue disks), and single no-slip HBC in water (red triangles). Each data point corresponds to the average from three independent simulations, and the error bars correspond to the standard deviation. (b) Specific viscosity of a multiparticle suspension in water as a function of the solid fraction ϕ_s of slip (blue disks) or no-slip (red triangles) HBC for Pe = 62. Solid lines are linear fits to the data in the limit of a low volume fraction, respectively, $\eta_{sp}/\phi_s = 3$ (red) and $\eta_{sp}/\phi_s = 0.77$ (blue).

performs continuous rotations, in agreement with Jeffery's prediction for rigid axisymmetric particle [Fig. 3(b)]. For the largest Pe, we measure a period of rotation of $\mathcal{T} \approx 130$ ps, only about 30% lower than Jeffery's prediction $\mathcal{T} = 2\pi\dot{\gamma}^{-1}(k_e + k_e^{-1}) = 180$ ps. The average orientation angle is $\chi \approx 0$ and the degree of alignment $\Delta n''/\Delta n''_{max} \to 0.4$ as Pe $\to \infty$ [Figs. 2(a) and 2(b)]. Such intermediate value of $\Delta n''/\Delta n''_{max}$ reflects the fact that the molecule spends most of its rotational period aligned with the flow near $\chi \approx 0$. Again, the agreement between MD and the model with $k_e = 0.4$ is rather good. While the condition $\lambda < b$ is unlikely to occur for atomically thin pristine graphene-like particles in common solvents, $\lambda < b$ is possible for graphene-oxide platelets with a large enough degree of oxidation [12], as well as for other atomically heterogeneous platelets (e.g., clays [47]), because of a reduction in the slip length.

B. Viscosity measurement

The dynamics of a suspended molecule or particle affects the viscosity of a suspension, and measuring the viscosity could be a way of inferring the average orientation of a HBC experimentally. Using molecular dynamics simulations, we measure the wall shear stress τ_w, and from the expression $\eta = \tau_w/\dot{\gamma}$ we evaluate the specific viscosity of the suspension $\eta_{sp} = (\eta - \eta_0)/\eta_0$, where η_0 is the pure solvent viscosity. For a single no-slip HBC in water, we do not see strong evidence of a variation of η_{sp} with the Péclet number [red triangles in Fig. 4(a)]. For Pe > 10, η_{sp} is approximately constant with $\eta_{sp} \approx 0.11$. This result compares reasonably well with an asymptotic expression for oblate spheroids valid in the limits $b/a \to 0$ and Pe $\to \infty$ [48]. Using $b/a = 0.31$ and a solid fraction $\phi_s = 0.03$, this expression predicts $\eta_{sp} \sim \phi_s(3.183 - 1.792\, b/a) = 0.08$. For a single HBC with slip, however, $\eta_{sp} \approx 0.04\ \forall$ Pe, a significant reduction with respect to the no-slip case [blue disks in Fig. 4(a)]. The dilute theory for suspensions of force- and torque-free particles [49] suggests two possible causes for the reduction in viscosity: the reduced friction at the particle-solvent interface and the change in the average orientation of the particles. In the diluted limit, the specific viscosity of a suspension of no-slip particles with orientation confined to the flow-gradient plane can be written as [9,48,50]

$$\eta_{sp} = \phi_s\left(\frac{A}{2}\langle 1 - \cos 4\varphi\rangle + B + CD_r\langle \sin 2\varphi\rangle\right), \tag{8}$$

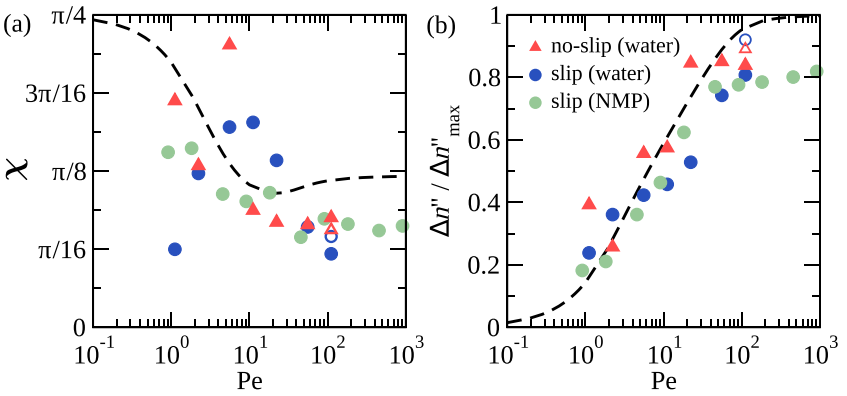

FIG. 5. (a) Average orientation angle χ and (b) degree of alignment $\Delta n''/\Delta n''_{\max}$ for varying Pe and multiple HBCs ($N = 16$): slip HBCs (blue disks) and no-slip HBCs (red triangles) in water; slip HBCs in NMP (green disks). Dashed lines are the theory for $N = 1$ [Eqs. (4)–(6)] and $k_e = 0.4i$. Open symbols correspond to results obtained using the Lees-Edwards boundary condition.

where A, B, and C are dimensionless coefficients, and $\langle \ldots \rangle$ indicates an average over all the particles in the suspension. The terms in the closed brackets in Eq. (8) are minimized when the particles are aligned indefinitely with time in the direction parallel to the shear flow field. In other words, a particle instantaneously aligned with the flow causes, on average, a smaller disturbance to the surrounding flow, as compared with a particle that continuously rotates. The coefficients A and B are obtained by calculating the first moment of the hydrodynamic traction on the surface of the particle, and hence depend on the particle geometry and on the slip length. For a given orientation, a reduction in tangential friction can thus lead to a reduction in viscosity by reducing the values of A and B.

C. Multiple solute particles

Particle-particle interactions (hydrodynamic and nonhydrodynamic) have a large effect on the orientation of a particle and, in turn, on the effective viscosity of the particle-solvent mixture. To investigate multiparticle effects with our solute molecules, we performed simulations with up to $N = 16$ HBCs in the computational domain of size $L_x \times L_y \times L_z \approx 3 \times 3 \times 7$ nm^3. The corresponding number density is $n = 0.25$ nm^{-3} and the solid fraction is $\phi_s \approx 0.4$. We measure the specific viscosity of the suspension of no-slip HBCs for fixed Pe $= 62$. We find a linear increase of η_{sp} with ϕ_s for $\phi_s < 0.1$, with $\eta_{sp}/\phi_s \approx 3$ [Fig. 4(b)]. For the slip HBCs, the increase is also linear for $\phi_s < 0.1$, but the slope is significantly reduced with respect to the no-slip case $\eta_{sp}/\phi_s \approx 0.45$. For ϕ_s larger than 0.1, the effective viscosity grows more than the linear prediction in the case of no-slip HBCs. This is expected from studies of no-slip particulate suspensions, and known to be a consequence of particle-particle interactions [51]. However, in the case of the slip HBCs, for ϕ_s larger than 0.1 the effective viscosity grows less than linearly. A possible explanation for this reduction in viscosity is the inhomogeneous distribution of HBCs in the wall-normal direction. For this concentration regime, visualizations indicate an average deficit of HBCs near the walls accompanied by the dynamic formation and breakup of predominantly horizontally aligned HBC clusters near the center of the box (Fig. S6 [22]). We speculate that this highly heterogeneous distribution of HBCs, together with the large slip length at the HBC-fluid interfaces, can be responsible for the observed reduction in viscosity. Overall, the larger ϕ_s the larger the viscosity differences between the slip and no-slip cases.

The dynamics of HBCs in water for $N = 16$ shows a nonmonotonic variation of χ with Pe, with a maximum for Pe $=$ Pe$^* \sim 10$ (Fig. 5). For Pe $\ll$ Pe*, we observe a decrease in χ with respect to

the $N = 1$ case. For $\mathrm{Pe} \gg \mathrm{Pe}^*$, the rotational dynamics is qualitatively similar to the dilute regime; the HBCs are on average aligned at a small angle with respect to the flow direction as for $N = 1$, although the values of χ and $\Delta n''/\Delta n''_{\max}$ are smaller than for $N = 1$ (Fig. 5). We attribute this behavior to the formation of clusters of HBCs (see snapshots in Fig. S3 [22]). For $\mathrm{Pe} \ll \mathrm{Pe}^*$, a single large cluster of stacked HBCs forms, which leads to a decrease in χ with respect to the $N = 1$ case. However, the observed decrease in χ must be interpreted with caution, first because of the large corresponding variance (or small values of $\Delta n''/\Delta n''_{\max}$), and second because the formation of a large cluster is associated with relaxation times that are larger than the duration of MD simulations. For $\mathrm{Pe} \gg \mathrm{Pe}^*$, hydrodynamic forces are able to overcome the relatively strong interparticle adhesive forces, leading to the dynamic formation and breakup of small clusters of HBCs.

The shear rate value $\dot{\gamma}^*$ above which hydrodynamic forces are sufficiently large to break small stacks of aligned particles can be estimated as $\dot{\gamma} \sim \frac{\Delta\mathcal{E}}{\eta a} f(\frac{\lambda}{a}, \frac{b}{a})$, where $\Delta\mathcal{E}$ is the change in surface energy associated with the separation in a liquid of two solid molecular layers, and f is a nondimensional function that is typically $O(1)$ [52]. From this expression, the Pe number corresponding to $\dot{\gamma}^*$ is seen to be independent of the fluid viscosity and to scale as $\mathrm{Pe}^* \sim a^2 \Delta\mathcal{E} f / k_B T$. For HBCs in water, using $f = 1$ and $\Delta\mathcal{E} = 60\ \mathrm{mJ/m^2}$, we get $\mathrm{Pe}^* = 9$ [52]. In the case of HBCs in NMP, $\Delta\mathcal{E} = 4\ \mathrm{mJ/m^2}$ and $\mathrm{Pe}^* = 0.6$ [52]. Compatibly with this estimate, simulations with $N = 16$ HBCs in NMP show no clustering, even at the lowest Pe simulated (Fig. 5). The value of χ is only slightly reduced compared with the case $N = 1$ for intermediate values of Pe. For Pe in the range 10^2–10^3, the values of χ for $N = 1$ and 16 are practically identical. The results suggest that in absence of clustering and for a volume fraction $\phi_s \approx 0.4$, the rotational dynamics of multiple HBCs is qualitatively similar to the case $N = 1$.

To evaluate the effect of particle-particle interaction in the case of HBCs with a modified solid-liquid energy of interaction, we performed simulations with $N = 16$ no-slip HBCs. Due to the large solid-liquid surface energy characterizing the no-slip HBC boundaries, no-slip HBCs do not agglomerate even for $\mathrm{Pe} \approx 1$. In contrast with the case $N = 1$, the results show that when $N = 16$, no-slip HBCs align with the flow at large Pe (Fig. 5). This behavior is likely due to short-range hydrodynamic and contact interactions, as previously shown for disk-like particles of moderate aspect ratios ($b/a = 0.15$–0.33) composed of spherical beads [53]. The comparison between the slip and no-slip cases for $N = 16$ suggests that, in this regime, the impact of hydrodynamic slip on the orientation of the HBCs is small. Although in our multiparticle simulations the influence of the proximity of the two shearing walls on the orientation can not be completely ruled out, results obtained using Lees-Edwards boundary conditions [54] to simulate an effectively unbounded suspension lead to the same results as those obtained with the bounded suspension, suggesting that the effect of the walls is negligible (open symbols in Fig. 5).

III. CONCLUSION

In conclusion, we have demonstrated a large effect of hydrodynamic slip on the rotational dynamics of a nanographene, HBC, in shear flow. In particular, at large Péclet number, our molecular dynamics results show that HBCs align with a constant orientation angle instead of performing the classical periodic orbits predicted by Jeffery's theory. Steady orientation in shear flow has been previously observed for vesicles due to the so-called tank-threading motion [55], for flexible filaments assuming highly folded shapes [56], and for rigid no-slip rings with specific cross sections [57], but the microphysics leading to orientation in these systems is markedly different from that characterizing our system. Theoretical predictions by a one-dimensional Fokker-Planck model for the trend of the average orientation angle χ and degree of alignment $\Delta n''/\Delta n''_{\max}$ of a single solute molecule as function of Pe agree well with MD data for $1 < \mathrm{Pe} < 10^3$ (see Fig. 2). We have also quantified changes in orientational statistics due to particle-particle interaction between several HBCs. Our results suggest that in absence of clustering and for a volume fraction $\phi_s \approx 0.4$, the rotational dynamics of multiple HBCs is qualitatively similar to the case $N = 1$. Our results also show a strong effect of hydrodynamic slip on the viscosity of the suspension of HBCs in water; for

a solid fraction $\phi_s \approx 0.4$, the effective viscosity of a suspension with slip solute molecules is about 40 % lower than with no-slip solute molecules. This study allows for a better understanding of the behavior of plate-like macromolecules and particles, including graphene-like colloids, and should encourage investigations on the effect of slip on the dynamics of solute molecules under shear flow. Controlling macroscopic properties of complex fluids such as graphene suspensions is critical to deliver on the promise of two-dimensional materials [42,58–60]. Furthermore, HBCs are foreseen as building blocks for the realization of active layers for transistors [61], supercapacitors [62], and photovoltaic cells [63].

ACKNOWLEDGMENTS

This project has received funding from the European Research Council (ERC) under the European Union's Horizon 2020 research and innovation programme (Grant Agreement No. 715475). This research utilized Queen Mary's Apocrita HPC facility, supported by QMUL Research-IT.

[1] O. Diat, D. Roux, and F. Nallet, Effect of shear on a lyotropic lamellar phase, J. Phys. II France **3**, 1427 (1993).
[2] Z. Fan and S. G. Advani, Characterization of orientation state of carbon nanotubes in shear flow, Polymer **46**, 5232 (2005).
[3] C. M. Schroeder, R. E. Teixeira, E. S. G. Shaqfeh, and S. Chu, Characteristic Periodic Motion of Polymers in Shear Flow, Phys. Rev. Lett. **95**, 018301 (2005).
[4] D. Saintillan, Rheology of active fluids, Annu. Rev. Fluid Mech. **50**, 563 (2018).
[5] E. Di Stasio and R. De Cristofaro, The effect of shear stress on protein conformation: Physical forces operating on biochemical systems: The case of von Willebrand factor, Biophys. Chem. **153**, 1 (2010).
[6] R. G. Winkler, Conformational and rheological properties of semiflexible polymers in shear flow, J. Chem. Phys. **133**, 164905 (2010).
[7] R. G. Cox, The motion of long slender bodies in a viscous fluid Part 1. General theory, J. Fluid Mech. **44**, 791 (1970).
[8] V. Singh, D. L. Koch, G. Subramanian, and A. D. Stroock, Rotational motion of a thin axisymmetric disk in a low Reynolds number linear flow, Phys. Fluids **26**, 033303 (2014).
[9] G. B. Jeffery, The motion of ellipsoidal particles immersed in a viscous fluid, Proc. R. Soc. London **102**, 161 (1922).
[10] A. Sellier, Arbitrary Stokes flow about a fixed or freely-Suspended slip particle, Comput. Model. Eng. Sci. **96**, 159 (2013).
[11] J. Zhang, X. Xu, and T. Qian, Anisotropic particle in viscous shear flow: Navier slip, reciprocal symmetry, and Jeffery orbit, Phys. Rev. E **91**, 033016 (2015).
[12] C. Kamal, S. Gravelle, and L. Botto, Hydrodynamic slip can align thin nanoplatelets in shear flow, Nat. Commun. **11**, 2425 (2020).
[13] B. D. Leahy, D. L. Kock, and I. Colen, The effect of shear flow on the rotational diffusion of a single axisymmetric particle, J. Fluid Mech. **772**, 42 (2015).
[14] J. Marguerite Hughes, Y. Hernandez, D. Aherne, L. Doessel, K. Müllen, B. Moreton, T. W. White, C. Partridge, G. Costantini, A. Shmeliov, M. Shannon, V. Nicolosi, and J. N. Coleman, High quality dispersions of hexabenzocoronene in organic solvents, J. Am. Chem. Soc. **134**, 12168 (2012).
[15] G. Tocci, L. Joly, and A. Michaelides, Friction of water on graphene and hexagonal BN from ab initio methods: Very different slippage despite very similar interface structures, Nano Lett. **14**, 6872 (2014).
[16] E. Secchi, S. Marbach, A. Niguès, D. Stein, A. Siria, and L. Bocquet, Massive radius-dependent flow slippage in single carbon nanotubes, Nature (London) **537**, 210 (2016).
[17] S Plimpton, Fast parallel algorithms for short-range molecular-dynamics, J. Comput. Phys. **117**, 1 (1995).
[18] N. Schmid, A. P. Eichenberger, A. Choutko, S. Riniker, M. Winger, A. E. Mark, and W. F. Van Gunsteren,

Definition and testing of the GROMOS force-field versions 54A7 and 54B7, Eur. Biophys. J. **40**, 843 (2011).
[19] J. L. Abascal and C. Vega, A general purpose model for the condensed phases of water: TIP4P/2005, J. Chem. Phys. **123**, 234505 (2005).
[20] T. Darden, D. York, and L. Pedersen, Particle mesh Ewald: An N log(N) method for Ewald sums in large systems, J. Chem. Phys. **98**, 10089 (1993).
[21] Q. Lu and R. Luo, A Poisson-Boltzmann dynamics method with nonperiodic boundary condition, J. Chem. Phys. **119**, 11035 (2003).
[22] See Supplemental Material at http://link.aps.org/supplemental/10.1103/PhysRevFluids.6.034303 for a description of the simulation, a description of the rotational diffusion coefficient measurement, a description of the effective aspect ratio measurement, a description of the bending rigidity measurement, a description of the enforcement of the no-slip boundary condition, and Figs S1, S2, S3, S4, S5 and S6.
[23] J.-P. Ryckaert, G. Ciccotti, and H. J. C. Berendsen, Numerical integration of the cartesian equations of motion of a system with constraints: Molecular dynamics of n-alkanes, J. Comput. Phys. **23**, 327 (1977).
[24] A. K. Malde, L. Zuo, M. Breeze, M. Stroet, D. Poger, P. C. Nair, C. Oostenbrink, and A. E. Mark, An Automated force field Topology Builder (ATB) and repository: Version 1.0, J. Chem. Theory Comput. **7**, 4026 (2011).
[25] D. M. Huang, C. Cottin-Bizonne, C. Ybert, and L. Bocquet, Aqueous electrolytes near hydrophobic surfaces: Dynamic effects of ion specificity and hydrodynamic slip, Langmuir **24**, 1442 (2008).
[26] A. Ortega and J. G. De La Torre, Hydrodynamic properties of rodlike and dislike particles in dilute solution, J. Chem. Phys. **119**, 9914 (2003).
[27] A. Kharazmi and N. V. Priezjev, Molecular dynamics simulations of the rotational and translational diffusion of a Janus rod-shaped nanoparticle, J. Phys. Chem. B **121**, 7133 (2017).
[28] J. D. Sherwood, Resistance coefficients for Stokes flow around a disk with a Navier slip condition, Phys. Fluids **24**, 093103 (2012).
[29] C. J. Pipe, T. S. Majmudar, and G. H. McKinley, High shear rate viscometry, Rheol. Acta **47**, 621 (2008).
[30] S. S. Vadodaria, A. J. Onyianta, and D. Sun, High-shear rate rheometry of micro-nanofibrillated cellulose (CMF/CNF) suspensions using rotational rheometer, Cellulose **25**, 5535 (2018).
[31] N. K. Reddy, G. Natale, R. K. Prud'Homme, and J. Vermant, Rheo-optical analysis of functionalized graphene suspensions, Langmuir **34**, 7844 (2018).
[32] P. L. Frattini and G. G. Fuller, Rheo-optical studies of the effect of weak Brownian rotations in sheared suspensions, J. Fluid Mech. **168**, 119 (1986).
[33] F. P. Bretherton, The motion of rigid particles in a shear flow at low Reynolds number, J. Fluid Mech. **14**, 284 (1962).
[34] M. M. Tirado and J. G. De La Torre, Rotational dynamics of rigid, symmetric top macromolecules. Application to circular cylinders, J. Chem. Phys. **73**, 1986 (1980).
[35] C. Gardiner, *Handbook of Stochastic Methods: For Physics, Chemistry & the Natural Sciences* (Series in Synergetics (Springer, Berlin, 2004), Vol. 13.
[36] S. Kim and S. J. Karrila, *Microhydrodynamics: Principles and Selected Applications* (Dover, New York, 2013).
[37] E. J. Hinch and L. G. Leal, Time-dependent shear flows of a suspension of particles with weak Brownian rotations, J. Fluid Mech. **57**, 753 (1973).
[38] Q. Wang, Simulations of the bending rigidity of graphene, Phys. Lett. A **374**, 1180 (2010).
[39] V. N. Borysiuk, V. N. Mochalin, and Y. Gogotsi, Bending rigidity of two-dimensional titanium carbide (MXene) nanoribbons: A molecular dynamics study, Comput. Mater. Sci. **143**, 418 (2018).
[40] P. S. Lingard and R. L. Whitmore, The deformation of disc-shaped particles by a shearing fluid with application to the red blood cell, J. Colloid Interface Sci. **49**, 119 (1974).
[41] N. Quennouz, M. Shelley, O. Du Roure, and A. Lindner, Transport and buckling dynamics of an elastic fibre in a viscous cellular flow, J. Fluid Mech. **769**, 387 (2015).
[42] Y. Hernandez, V. Nicolosi, M. Lotya, F. M. Blighe, Z. Sun, S. De, I. T. Mcgovern, B. Holland, M. Byrne, Y. K. Gun'Ko, J. J Boland, P. Niraj, G. Duesberg, S. Krishnamurthy, R. Goodhue, J. Hutchison,

V. Scardaci, A. C. Ferrari, and J. N. Coleman, High-yield production of graphene by liquid-phase exfoliation of graphite, Nat. Nanotechnol. **3**, 563 (2008).
[43] R. D. Nelson and C. P. Smyth, Microwave absorption and molecular structure in liquids. LIX. The relation between dielectric relaxation, viscosity, and molecular size, J. Phys. Chem. **68**, 2704 (1964).
[44] M. A. González and J. L. F. Abascal, The shear viscosity of rigid water models, J. Chem. Phys. **132**, 096101 (2010).
[45] A. Henni, J. J. Hromek, P. Tontiwachwuthikul, and A. Chakma, Volumetric properties and viscosities for aqueous N-Methyl-2-pyrrolidone solutions from 25 °C to 70 °C, J. Chem. Eng. Data **49**, 231 (2004).
[46] C. Herrero, T. Omori, Y. Yamaguchi, and L. Joly, Shear force measurement of the hydrodynamic wall position in molecular dynamics, J. Chem. Phys. **151**, 041103 (2019).
[47] A. Boţan, B. Rotenberg, V. Marry, P. Turq, and B. Noetinger, Hydrodynamics in clay nanopores, J. Phys. Chem. C **115**, 16109 (2011).
[48] L. G. Leal and E. J. Hinch, The effect of weak Brownian rotations on particles in shear flow, J. Fluid Mech. **46**, 685 (1971).
[49] G. K. Batchelor, The stress system in a suspension of force-free particles, J. Fluid Mech. **41**, 545 (1970).
[50] E. J. Hinch and L. G. Leal, The effect of Brownian motion on the rheological properties of a suspension of non-spherical particles, J. Fluid Mech. **52**, 97 (1972).
[51] E. Guazzelli and J. F. Morris, *A Physical Introduction to Suspension Dynamics* (Cambridge University Press, Cambridge, 2011), Vol. 45.
[52] S. Gravelle, C. Kamal, and L. Botto, Liquid exfoliation of multilayer graphene in sheared solvents: A molecular dynamics investigation, J. Chem. Phys. **152**, 104701 (2020).
[53] Q. Meng and J. J. L. Higdon, Large scale dynamic simulation of plate-like particle suspensions. Part I: Non-Brownian simulation, J. Rheol. **52**, 1 (2008).
[54] A. W. Lees and S. F. Edwards, The computer study of transport processes under extreme conditions, J. Phys. C: Solid State Phys. **5**, 1921 (1972).
[55] S. R. Keller and R. Skalak, Motion of a tank-treading ellipsoidal particle in a shear flow, J. Fluid Mech. **120**, 27 (1982).
[56] Y. Liu, B. Chakrabarti, D. Saintillan, A. Lindner, and O. Du Roure, Morphological transitions of elastic filaments in shear flow, Proc. Natl. Acad. Sci. USA **115**, 9438 (2018).
[57] V. Singh, D. L. Koch, and A. D. Stroock, Rigid ring-shaped particles that align in simple shear flow, J. Fluid Mech. **722**, 121 (2013).
[58] A. Hirsch, J. M. Englert, and F. Hauke, Wet chemical functionalization of graphene, Acc. Chem. Res. **46**, 87 (2013).
[59] E. B. Secor, P. L. Prabhumirashi, K. Puntambekar, M. L. Geier, and M. C. Hersam, Inkjet printing of high conductivity, flexible graphene patterns, J. Phys. Chem. Lett. **4**, 1347 (2013).
[60] D. W. Johnson, B. P. Dobson, and K. S. Coleman, A manufacturing perspective on graphene dispersions, Curr. Opin. Colloid Interface Sci. **20**, 367 (2015).
[61] W. Pisula, A. Menon, M. Stepputat, I. Lieberwirth, U. Kolb, A. Tracz, H. Sirringhaus, T. Pakula, and Klaus Müllen, A zone-casting technique for device fabrication of field-effect transistors based on discotic hexa-perihexabenzocoronene, Adv. Mater. **17**, 684 (2005).
[62] L. Qin, Y. Zhang, X. Wu, L. Nian, Z. Xie, L. Liu, and Y. Ma, In situ electrochemical synthesis and deposition of discotic hexa-peri-hexabenzocoronene molecules on electrodes: Self-assembled structure, redox properties, and application for supercapacitor, Small **11**, 3028 (2015).
[63] C. J. Brabec, N. S. Sariciftci, and J. C. Hummelen, Plastic solar cells, Adv. Funct. Mater. **11**, 15 (2001).